HHS Public Access

Author manuscript

Rep U S. Author manuscript; available in PMC 2015 December 24.

Published in final edited form as:

Rep U S. 2015 ; 2015: 216–221. doi:10.1109/IROS.2015.7353377.

A Robotic System for Actively Stiffening Flexible Manipulators

Paul M. Loschak [Student Member, IEEE], **Stephen F. Burke**, **Emiko Zumbro**, **Alexandra R. Forelli**, and **Robert D. Howe [Fellow, IEEE]**

Harvard Paulsen School of Engineering and Applied Sciences, Harvard University, Cambridge, MA, USA

Paul M. Loschak: Loschak@seas.harvard.edu

Abstract

A system for actively changing the stiffness of a long, thin, flexible robotic manipulator has been designed for cardiologists to use in a range of diagnosis and treatment procedures. Low-stiffness manipulators, such as catheters, are ideal for steering through vasculature with low risk of tissue injury. However, such instruments are not well-suited for applying force to tissue. The proposed system solves this problem by using a series of bead-shaped vertebrae containing pull wires to actively change the stiffness of the catheter, similar to gooseneck surgical retractors. Individual wires steer the catheter to a desired location. All wires are then tensioned to create friction between each vertebra and prevent sliding, therefore resisting motion. While this design concept has been implemented manually in various settings for decades, fine robotic control of the friction and stiffness of the system relies on a thorough understanding of the friction properties between vertebral segments. We have developed an analytical model to understand the interactions between vertebrae and determine the relationships between system parameters and the overall stiffness of the catheter. Experiments validated the calculations from the model and the functionality of the system by applying known loads to the tip of the catheter and measuring the catheter displacement. The catheter stiffness was measured to range from 100 N/m to 800 N/m, which is sufficient for performing many surgical tasks on tissue. This system can be useful in minimally invasive procedures involving direct instrument contact with tissue by improving accuracy, safety, and work flow.

I. INTRODUCTION

Progress in minimally invasive surgery has seen advances in long, thin, flexible manipulators which are actuated from outside the patient. Cardiac catheterization is an example of a minimally invasive method for diagnosis and treatment of a variety of conditions including atrial fibrillation, valve replacement, and biopsy [1]. Cardiac catheters can be inserted into the patient through femoral vessels and navigated through the vasculature to the heart. Cardiac catheters are typically equipped with either sensors for recording measurements or end effectors for interacting with tissue, such as highly conductive metal tips for radiofrequency ablation. In some instances it is important for catheters to have very low stiffness (to avoid damaging tissue), and in other instances stiffness is important for applying high forces (such as in biopsy sampling).

Cardiac catheters are manufactured with a wide variety of diameters, materials, and stiffness properties for different medical applications. Soft flexible catheters with low stiffness are ideal for navigating through the vasculature or steering through heart chambers, but poor for applying forces to tissue. At present, to apply force to tissue it is necessary to remove the flexible catheter and replace it with a stiffer catheter. Stiffer catheters are useful for applying forces to tissue, but increase the risk of injuring heart structures or perforating through the heart wall during navigation. Switching catheters requires time and effort, and it reduces the positioning accuracy which was achieved during navigation with the flexible catheter.

Methods for achieving variable stiffness manipulators of a larger diameter (endoscopes) have been proposed [2], [3], [4], [5], but these strategies do not succeed when scaled down to smaller diameters. Researchers have examined hybrid actuation methods and flexible manipulator stiffnesses [6], [7]. A research prototype for an actively steering catheter uses the interactions between two friction-locking bead designs to assist in steering through restricted areas [8]. Another research prototype uses wires and rotating links to affect the stiffness of the manipulator when acted upon by outside forces [9]. The patent literature also contains several examples of inventions towards variable stiffness flexible manipulators [10], [11], [12]. While many of these prototypes have demonstrated promising results, we are investigating a friction-based method which enables higher stiffnesses.

The device described in [10] serves as the primary inspiration for our analytical contributions. This flexible surgical retractor contains cables through a central channel. Tightening the cable increases friction between vertebral segments, thereby increasing the stiffness of the instrument. It is our goal to build a catheter-sized version of this device in which it is possible to robotically tighten the cables, thereby automatically adjusting the stiffness to a desired amount.

This paper presents the design, implementation, and testing of a flexible manipulator capable of actively changing stiffness properties quickly and repeatedly. First, the system design requirements and adaptation to steerable cardiac catheterization are described. Next, analytical models are derived for describing: (a) the design of the catheter for achieving an appropriate workspace, (b) the stiffness properties of the catheter due to materials, (c) the amount of static friction between vertebrae as a function of cable tension, and (d) the amount of external force which causes slippage. The stiffening module is then integrated with a robotic actuation platform and experiments are conducted to test its stiffness. The work presented here has the potential to increase accuracy for minimally invasive procedures, improve clinical workflow, and reduce procedure times.

II. Methods

The robotic catheter system presented here must be able to navigate the catheter tip to a desired position and then withstand external force. The system must therefore shift between two modes: steering mode (low stiffness) and force application mode (high stiffness). In steering mode the catheter tip must have low stiffness to enable navigation. In force application mode the stiffness should reach a minimum of 500 N/m, so that a force of 1.5 N against cardiac tissue will deflect the catheter tip by less than 3 mm [13]. The catheter tip

position must remain stationary while switching between states. This is a safety precaution to prevent the obstruction of cardiac motion or damage to structures while switching modes.

Actively increasing the stiffness of a long, thin, flexible plastic tool poses a significant design challenge. Several methods inspired by prior art for stiffening thin flexible manipulators were explored: shape memory alloys, inter-locking tooth mechanisms, granular jamming, and hydraulics [2], [3], [4], [5]. The chosen design strategy for varying catheter stiffness, based on [10], used a series of plastic vertebrae with four channels for pull wires spaced 90° apart (Fig. 1). Channels were shaped conically to increase the pull wire range of motion. Tensioning all pull wires causes the vertebrae to press against each other. Friction forces prevent sliding at interfaces between vertebrae, thereby increasing the overall stiffness of the catheter.

III. Modeling

A. Workspace Calculations

Each vertebra features a tip radius that is slightly larger than the radius of the actual bead. This allows the vertebrae to slide and rotate within some allowable range. Fig. 2 (*left*) shows the mating geometry between two vertebrae. Each vertebra is capable of sliding by the maximum angle φ before colliding with the cylindrical side of the vertebra. The maximum angle is solved by

$$\phi = 2\cos^{-1}\left(\frac{D}{2R}\right) \quad (1)$$

where *D* is the vertebra diameter and *R* is the tip radius. Fig. 2 (*right*) shows a black dot at the center of each tip circle. These dots are used to calculate the location of the vertebrae in terms of *z* (height) and *x* (distance from the initial centerline). For *N* vertebrae, the final position of the most distal point on the catheter is given by

$$z_N = -R\sin\frac{\phi}{2} + L\left[\sum_{0}^{N-1}\cos(N\phi)\right] + R\cos((N-1)\phi)$$

$$x_N = L\left[\sum_{1}^{N-1}\sin(N\phi)\right] + R\sin((N-1)\phi). \quad (2)$$

This workspace model provides insight into the design of the catheter. A longer vertebral length is advantageous for a larger workspace at the cost of increasing the turning radius. The dimensions of the diameter of the vertebrae relative to the tip radius must be tuned to reach an adequate bending angle. Fig. 3 plots the maximum deflection as a function of *D/R*. The max diameter is limited to $D \leq 2R$. The geometric parameters used for the preliminary tests in this work are shown in Fig. 4.

B. Vertebral Contact Model

Lateral force applied to the tip of the catheter causes vertebrae to rotate with respect to each other. To understand this relationship, we analyze the contact between two vertebrae and develop appropriate models. Examination of stiffness data shows two types of motion during stiffening tests (Fig. 5): (A) elastic structural displacement and (B) sliding displacement. As forces are applied to the catheter tip a small amount of elastic displacement occurs in the mechanical structure of the system due to pull wire stretch, pull wires shifting inside channels, vertebral compression, plastic effects, defects in vertebrae, fasteners, etc. (schematic line A in Fig. 5). As higher forces are applied to the distal vertebra, a moment about the proximal vertebra overcomes the static Coulomb frictional moment between surfaces and causes the spherical surfaces on each vertebra to begin sliding (schematic line B in Fig. 5). The stiffness is significantly reduced during sliding, but the slope of the stiffness curve remains positive due to additional structural deformation. Removal of the tip force then causes the elastic deformations to relax (schematic line C in Fig. 5).

C. Elastic Structural Displacement

Catheter motion due to elastic structural displacement can be modeled through the principles of virtual work. For the simplest case of a catheter with two vertebrae, a lateral force F can be applied to the distal vertebra in order to create a small lateral displacement Δx. These quantities are related by stiffness K_{tip}. The resulting angular displacement, $\Delta\theta$, occurs as the vertebrae are made to pivot about the corner of contact (Fig. 6). The structural elements of the system comply elastically as the pull wire is slightly elongated, and the sum of these effects is modeled by a spring with stiffness k_{ES}. The work applied to the catheter tip, W_{app}, is calculated by multiplying the applied tip force, F, with the catheter tip displacement along the arc created by the pivot point. This is equated with the work done by the elastic structural spring with stiffness k_{ES} by

$$W_{app}=F\Delta x=\frac{1}{2}k_{ES}\Delta s^2, \quad (3)$$

where Δs is the elastic structural deformation of the system. By using small angle approximations in (4) it is possible to calculate K_{tip} as a function of L, R, and k_{ES} as in

$$\Delta x \approx (L+R)\Delta\theta, \Delta s \approx L\Delta\theta \quad (4)$$

$$K_{tip}=\frac{F}{\Delta x}=\frac{F}{(L+R)\Delta\theta}=\frac{k_{ES}L^2}{2(L+R)^2}. \quad (5)$$

The slope of the stiffness curve in elastic structural deformation, K_{tip}, is a constant which is dependent on vertebral geometry and k_{ES}.

D. Sliding Displacement

If the applied force increases to create a rotational moment about the vertebra which exceeds the threshold of the friction moment, then the vertebra will begin sliding. This threshold of maximum static friction can be estimated by forming a model to relate the vertebral

parameters with the friction moment. Once sliding has occurred, sliding friction is not modeled analytically. Dynamic effects are neglected because the catheter is designed to remain stationary during stiffness changes. The convex spherical protrusion on the tip of each vertebra mates with the concave spherical intrusion at the tail of the next distal vertebra. High tension forces from the pull wires compress these vertebral surfaces together and create static friction. This interaction can be approximated as a ball in socket problem, in which a Coulomb frictional moment resists rotation of the vertebrae. An estimate of the frictional moment will be calculated by assuming that the two spherical surfaces contact each other as a point force. A more accurate calculation of the friction moment could be obtained by using the techniques described in [14] to represent the interaction as a surface with Hertzian contact. However, the point force assumption is sufficient in this case.

Fig. 7 shows a 3D force *F* applied to one vertebra. The force is applied at the location (l_x, l_y, l_z) with angle *a* rotation from the *y*-axis and angle *b* rotation from the *x*-axis. The spherical surface of the vertebra presses against the adjoining vertebra at the location (n_x, n_y, n_z). The adjoining vertebra is not shown in Fig. 7. The total tension in the pull wires, *T*, acts at the location of the point force. The normal force, *N*, points towards the center of the sphere. The directionality of *N* is known to be angle *c* rotation from the *y*-axis and angle *d* rotation from the *x*-axis. The third force acting on the system is the friction force, μ*N*, which occurs at the same location as *N* and has directionality angle *e* from the *z*-axis and angle *f* from the *x*-axis. The constant μ represents the static coefficient of friction for the vertebra material. The angles *c* and *d* are equal to θ and φ as in [14], and these quantities are known by the sensor reporting the current location of the vertebrae. The location of *N* can be related to θ and φ by

$$c=\theta, d=\phi, n_x=Rsin\theta cos\phi$$

$$n_y=-Rcos\theta, n_z=Rsin\theta sin\phi. \quad (6)$$

Angles *a*, *b*, and force *F* are known quantities during experiments. The remaining unknown quantities are angles

$$\sum F_x: Fs_ac_b - Ns_cc_d+\mu Ns_ec_f+Ts_cc_d=0 \quad (7)$$

$$\sum F_y: -Fc_a+Nc_c+\mu Nc_e - Tc_c=0 \quad (8)$$

$$\sum M_x: Fc_al_z+Fs_as_bl_y-N_{c_c}n_z+Ns_cs_dn_y+\mu Ns_es_fn_y-\mu Nc_en_z+Tc_cn_z-Ts_cs_dn_y=0 \quad (9)$$

$$\sum M_z: -Fc_bs_al_y-Fc_al_x-Ns_cc_dn_y+Nc_cn_x+\mu Nc_en_x+\mu Ns_ec_fn_y+Ts_cc_dn_y-Tc_cn_x=0 \quad (10)$$

$$e=cos^{-1}\left[\frac{Tc_c+Fc_a-Nc_c}{\mu N}\right] \quad (11)$$

$$f=tan^{-1}\left[\frac{Fc_al_z+Fs_as_bl_y+Ns_cs_dn_y-Fc_an_z-Ts_cs_dn_y}{-Fc_bs_al_y-Fc_al_x-Ns_cc_dn_y+Fc_an_x+Ts_cc_dn_y}\right] \quad (12)$$

$$Fc_bs_a-Nc_ds_c+Tc_ds_c+\frac{N\mu\sqrt{1-\left(\frac{Fc_a-Nc_c+Tc_c}{N\mu}\right)^2}}{\sqrt{\left(\frac{Fc_al_z+Fs_as_bl_y-FRc_as_ds_c-NRc_cs_ds_c+RTc_cs_ds_c}{Fc_al_x+Fc_bs_al_y-FRc_ac_ds_c-NRc_dc_cs_c+RTc_dc_cs_c}\right)^2+1}}=0 \quad (13)$$

e, *f*, and normal force *N*, which must be solved in order to calculate the friction moment. The first step is to calculate the sum of the forces and moments in (7)–(10), where s_a =sin*a* and c_a =cos*a*. The sum equations are then combined in order to solve for *e* and *f* in terms of *N*, resulting in (11) and (12). Next, (11)–(12) can be substituted into (7) to obtain (13), from which *N* can be solved. The last step relates the friction moment, the threshold above which the vertebrae will slide, as

$$M_{friction}=R\times F_{friction}=R\mu N. \quad (14)$$

IV. Experiments

A. Robot Measurement System

A robotic system was designed to manipulate the variable stiffness catheter (Fig. 8). In steering mode the catheter is navigated to desired positions automatically. The steering process has been demonstrated in prior work ([15], [16]) and will not be examined here. Once the catheter tip has reached the desired position, all pull wires are tensioned to stiffen the catheter at its current location. When desired, the pull wires are relaxed and the catheter is navigated to a new position. The test system consists of the catheter (3D-printed vertebrae), actuators, tension sensors, connection electronics, and an optical tracking system. Four high-torque stepper motors (Changzhou Songyang Machinery & Electronics, China) steer the four pull wires. The motors are connected to an Arduino microcontroller via two motor shields (Adafruit, USA). S-type 100 kg load cell tension sensors (Phidgets, Canada) are integrated into the robotic system for measuring cable tensions. The entire system is interfaced through Matlab (MathWorks, USA). A closed-loop controller actuates the steppers to reach desired tensions in each of the four pull wires.

A short catheter consisting of two vertebrae was connected to the robot system in order to isolate the effects of pull wire tension on one friction surface between two vertebrae. The robotic cardiac catheter stiffening system was used to increase the tension in the pull wires throughout a series of stiffness testing trials. A single axis load cell rated for 0–25 kg (Futek, USA) was used to apply force to the tip of the catheter and measure the amount of force applied. Position measurements of the catheter tip were recorded by a high-resolution optical tracking system with resolution 0.25 mm RMS (Claron Technology Inc., Canada). Position

measurements were recorded at roughly 30 Hz. A tracking fiducial measuring 1 by 2 cm was attached to the tip of the catheter. The force and displacement measurements were used to calculate the overall catheter stiffness.

B. Results - Elastic Structural

A set of data was collected by applying force to the tip of the catheter to create elastic deformation followed by sliding friction. All trials were conducted with the catheter in the straightened position. This section focuses on the stiffness properties of the elastic region in which static friction between vertebral surfaces prevents sliding, but structural deformations cause linearly elastic deformations to occur. The measurements of force and displacement were used to calculate the overall stiffness of this region by using (5) for a range of different pull wire tensions. The mean K_{tip} value was 9181.5 N/m (standard deviation 3869.8 N/m). The mean k_{ES} value was 2067.8 N/m (standard deviation 871.5 N/m).

The stiffness of the elastic structural deformation is related to compliance in the construction of the robot, the vertebrae, and elongation of the pull wires. A linear stress-strain relationship,

$$\sigma = \frac{T}{A} = E\varepsilon = \frac{E\Delta s}{L_1}, \quad (15)$$

is used to draw a comparison between the measured tip deflection and the measured pull wire tension forces, T, where σ is stress in the pull wires, A is pull wire cross sectional area, L_1 is pull wire length, and E is pull wire modulus of elasticity (Kevlar E = 70–110 GPa). All four pull wires are tensioned differently when a lateral force is applied to the catheter tip. The calculated forces on each pull wire are summed to result in T ranging from 0–40 N. This is on the same order of magnitude as the measured pull wire tension forces, therefore demonstrating that elastic structural deformation largely results from uniaxial pull wire strains.

C. Results - Sliding Friction

This section focuses on sliding contact between spherical vertebral surfaces. The applied forces were used to calculate the applied moment on the distal vertebra. Force vs. displacement curves are shown for three pull wire tension forces in Fig. 9. Applied moments as a function of the total pull wire tension for 46 trials are shown as ”X” marks in Fig. 10. As the pull wire tension force increases, the moment required to create sliding displacement trends upwards. This trend validates the model summarized in (14), represented by the line in Fig. 10, which was used to calculate the moment required to overcome static friction. The two-vertebrae catheter was then replaced with a full length catheter of ten vertebrae. The overall stiffness of the catheter before sliding is shown in Fig. 11. A linear fit (Stiffness = $8.80T + 197.5$) represents the trend with $R^2 = 0.84$.

V. Conclusion

The work presented here is an initial prototype of a robotic system which actively changes the stiffness of a flexible manipulator to resist deformations due to external forces. A force

applied to the tip of the manipulator causes elastic deformation and potentially sliding between vertebrae. Therefore, an analytical model was derived to calculate the stiffness of the manipulator as a function of vertebral geometry and pull wire tension. The stiffness in the initial elastic deformation region, K_{tip}, is a constant value related to the geometry of the vertebrae and the physical properties of the pull wires. The stiffness then decreases when the force applied to the tip of the catheter exceeds the static Coulomb friction between vertebral surfaces, thereby causing sliding to occur. The spherical contact friction moment model relates the pull wire tension to the max force before sliding occurs. The robotic system was constructed in order to measure the stiffness of the manipulator and validate the analytical model.

While this system successfully demonstrated the ability to stiffen a flexible manipulator, there are several improvements to address through future work. A biocompatible rubber or plastic sleeve must be placed around the catheter in order to make this instrument clinically feasible and it will be necessary to examine its effects on the manipulator. The workspace model accuracy can be improved by accounting for the conic holes in each vertebra. Elastic deformation in the manipulator could be reduced by replacing the pull wires and the vertebrae with a material of higher E. Future vertebrae will be fabricated using materials of greater friction coefficients in order to increase the stiffening capability of the catheter while reducing the burden on pull wire tension, which is advantageous for patient safety. A working channel will enable instruments, fluids, or wires to pass through the center of the manipulator. Lastly, the non-uniform forces between different vertebrae along the length of the catheter will cause differences in the friction properties. These effects must be analyzed.

The analytical model describing the stiffness of the flexible manipulator was successfully validated on the prototype robot system. The resulting system allows a user to navigate the manipulator to a target destination while compliant. The user can then increase tension on the pull wires, with the magnitude of the tension set to prevent vertebrae sliding below the maximum anticipated tip load. The tip stiffness up to the sliding limit is then determined by the structural stiffness of the wires and the robot, which can be designed to provide desired tip stiffness. It is expected that the clinician will use the catheter in the structural elastic deformation region, and if the maximum force is exceeded then the catheter will simply slide (which avoids exerting dangerous forces on tissue). A system for actively stiffening flexible manipulators may be useful for many minimally invasive procedures in which a clinician must exert varying forces against tissue.

ACKNOWLEDGMENT

The authors would like to thank Diego Porras, MD, for helpful discussions on cardiac catheterization, and the Harvard School of Engineering and Applied Sciences Undergraduate Teaching Labs for supporting senior thesis research projects.

Work is supported by the Harvard Paulsen School of Engineering and Applied Sciences, the American Heart Association Grant 15PRE22710043, and the US National Institutes of Health under grant NIH R01 HL073647 and NIH 1R21EB018938.

References

1. Baim, DS. Grossmans Cardiac Catheterization, Angiography, and Intervention. Lippincott Williams & Wilkins; 2005. p. 992
2. Rex DK, et al. Insertability and safety of a shape-locking device for colonoscopy. American Journal of Gastroenterology. 2005; 100:817–820. [PubMed: 15784024]
3. Jiang, A., et al. Design of a Variable Stiffness Flexible Manipulator with Composite Granular Jamming and Membrane Coupling; Proc. IEEE/RSJ Int Conf on Intelligent Robots and Systems; 2012. p. 2922-2927.
4. Zuo, S., et al. Medical Image Computing and Computer-Assisted Intervention. Vol. 6891. New York: Springer Berlin Heidelberg; 2011. Nonmetallic rigid flexible outer sheath with pneumatic shapelocking mechanism and double curvature structure; p. 169-177.
5. Cheng, NG., et al. Design and Analysis of a Robust, Low-cost, Highly Articulated Manipulator Enabled by Jamming of Granular Media; Proc. IEEE Int. Conf. Robotics and Automation; 2012. p. 4328-4333.
6. Stilli, A.; Wurdemann, H.; Althoefer, K. Shrinkable, stiffness controllable soft manipulator based on a bio-inspired antagonistic actuation principle; IEEE/RSJ Int Conf on Intelligent Robots and Systems; 2014. p. 2476-2481.
7. Ataollahi A, Karim R, Fallah AS, Rhode K, Razavi R, Seneviratne L, Schaeffter T, Althoefer K. 3-dof mr-compatible multisegment cardiac catheter steering mechanism. IEEE Transactions on Biomedical Engineering. 2013; 99
8. Chen, Y., et al. Multi-turn, Tension-stiffening Catheter Navigation System; Proc. IEEE Int. Conf. Robotics and Automation; 2010. p. 5570-5575.
9. Kim Y-J, Cheng S, Kim S, Iagnemma K. A Stiffness-Adjustable Hyperredundant Manipulator Using a Variable Neutral-Line Mechanism for Minimally Invasive Surgery. IEEE Trans. on Robotics. 2014; 30(2):382–395.
10. Michelson, GK. Gooseneck surgical instrument holder. U.S. Patent 5513827. 1996 May.
11. Saadat, V., et al. Shape lockable apparatus and method for advancing an instrument through unsupported anatomy. U.S. Patent 7041052. 2006 May.
12. Fugoso, ML., et al. Adjustable stiffness dilation catheter. U.S. Patent 5545138. 1996 Aug..
13. Wagner, CR., et al. Force Feedback in a Three-Dimensional Ultrasound-Guided Surgical Task; 14th IEEE Symp. Haptic Interfaces for Virtual Environment and Teleoperator Systems; 2006. p. 43-48.
14. Faraz, A., et al. J Engineering Mathematics. Vol. 40. Springer; 2001. Towards approximate methods of coulomb frictional moments in: I) revolute pin joints and II) spherical-socket ball joints; p. 283-296.
15. Loschak, PM.; Brattain, LJ.; Howe, RD. Automated Pointing of Cardiac Imaging Catheters; Proc. IEEE Int. Conf. Robotics and Automation; 2013. p. 5774-5779.
16. Loschak PM, et al. Algorithms for automated pointing of cardiac imaging catheters. Proc. MICCAI Workshop on Computer-Assisted and Robotic Endoscopy. 2014

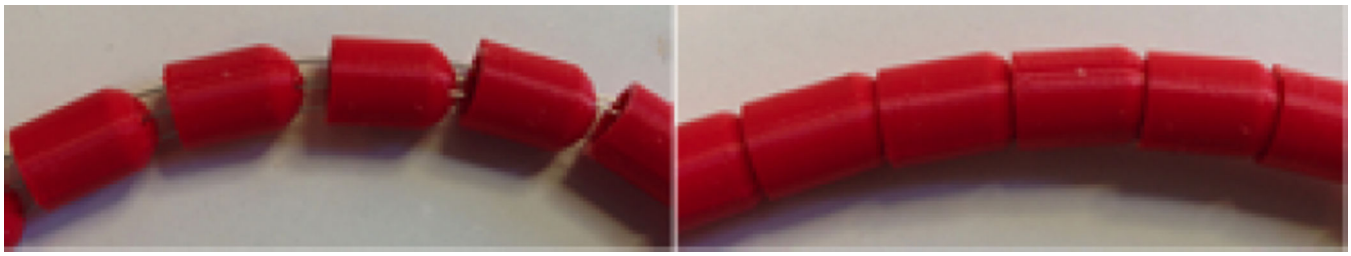

Fig. 1.

(*left*) Vertebrae are connected in series by pull wires. (*right*) Pull wires are tensioned to lock vertebrae in place.

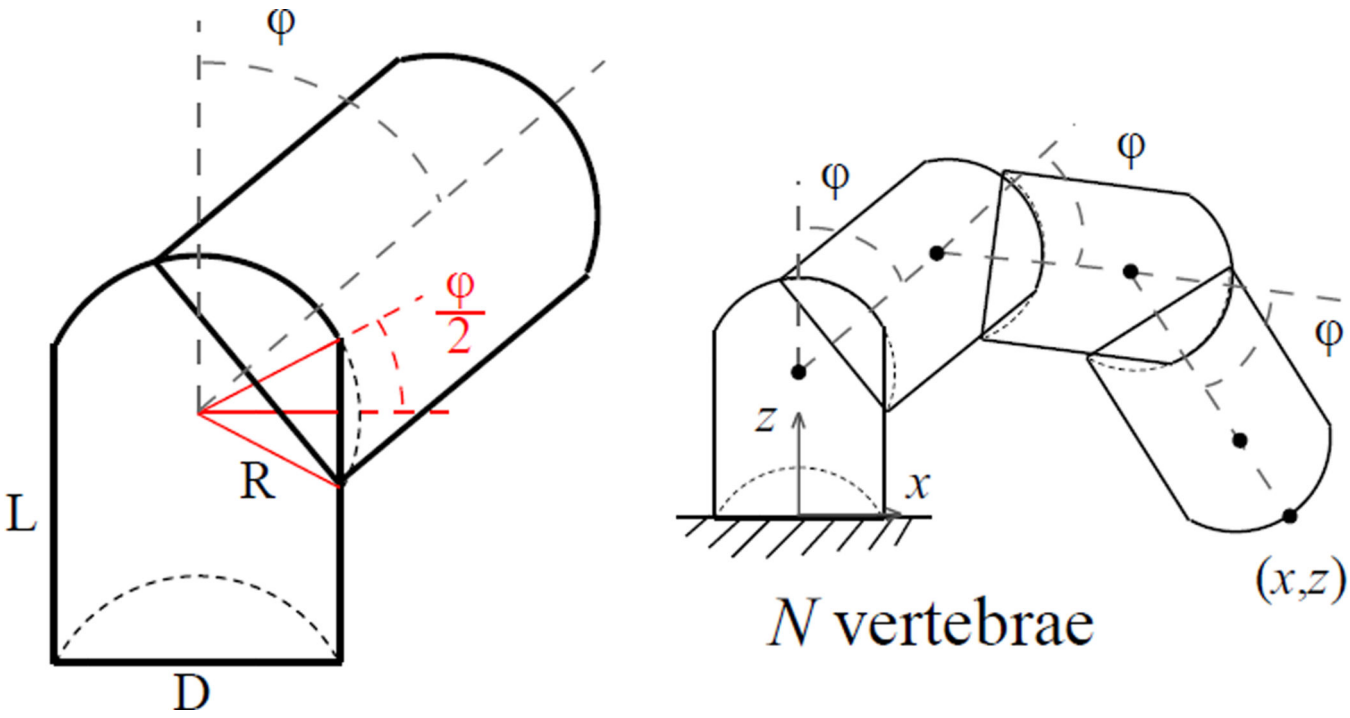

Fig. 2.
Diagram of geometric parameters and maximum catheter workspace.

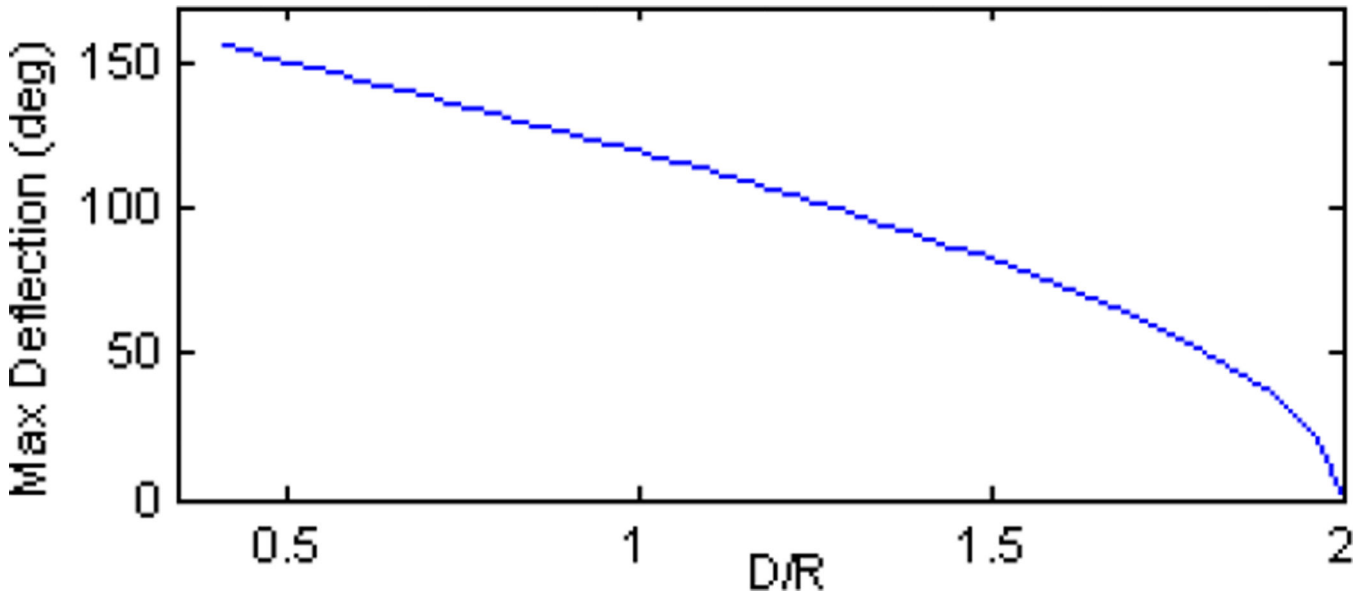

Fig. 3.

Max vertebrae rotation allowable (deg) as a function of the ratio between vertebrae diameter and tip radius.

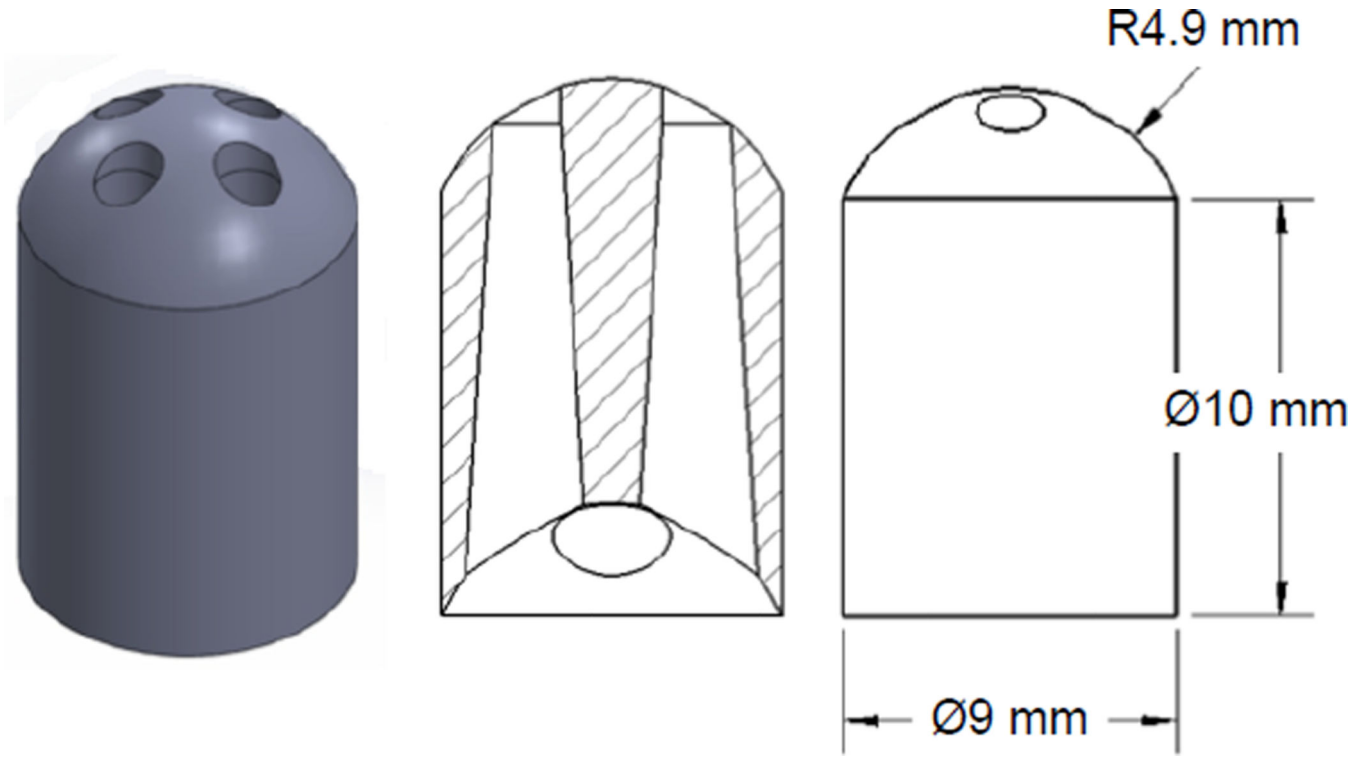

Fig. 4.
Vertebrae bead design and cross sectional view with dimensions.

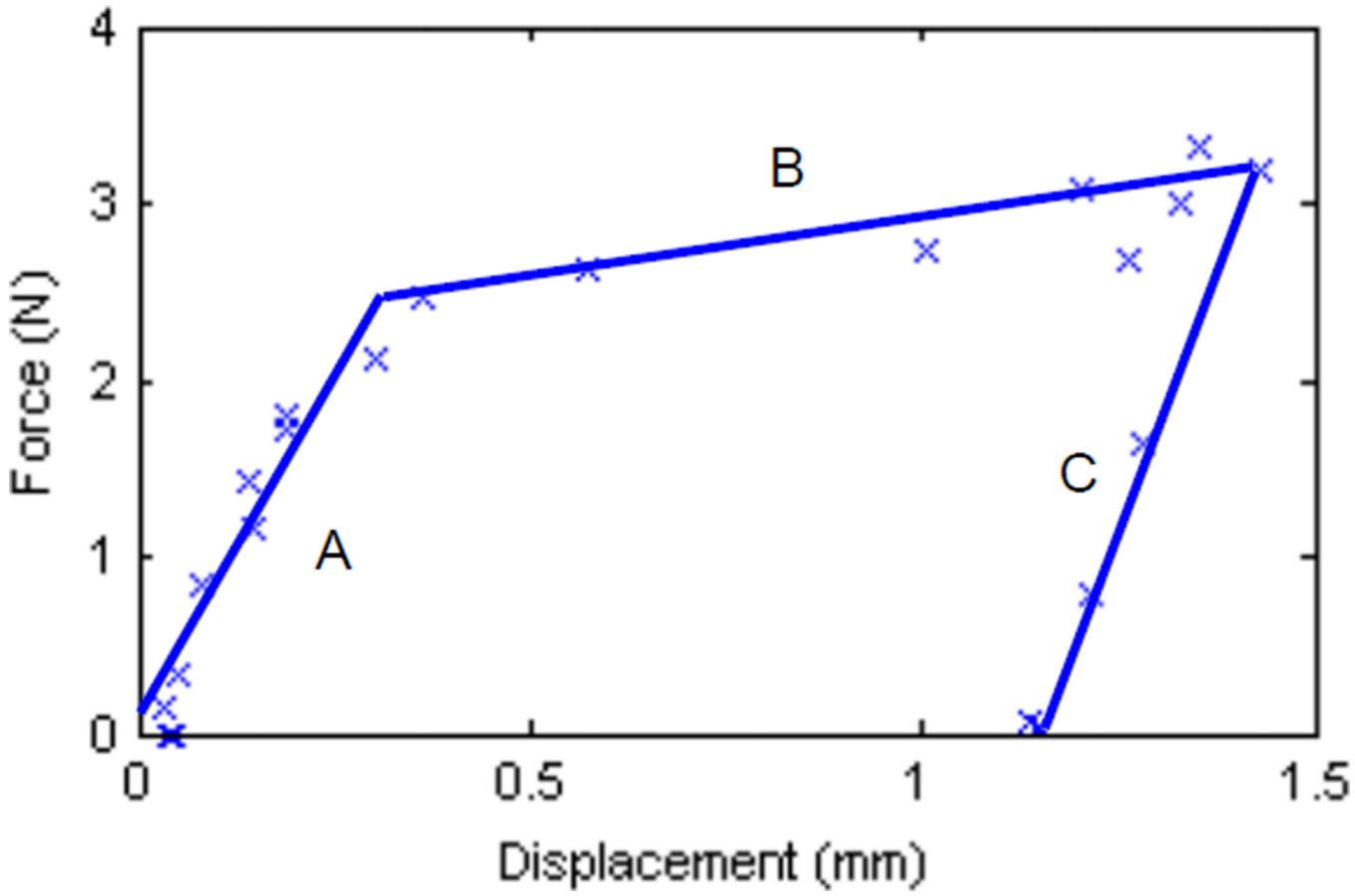

Fig. 5.

Typical force vs. displacement during catheter tip contact. Schematic line A results from elastic structural deformation. Schematic line B results from sliding friction. Schematic line C results from relaxation of elastic deformation.

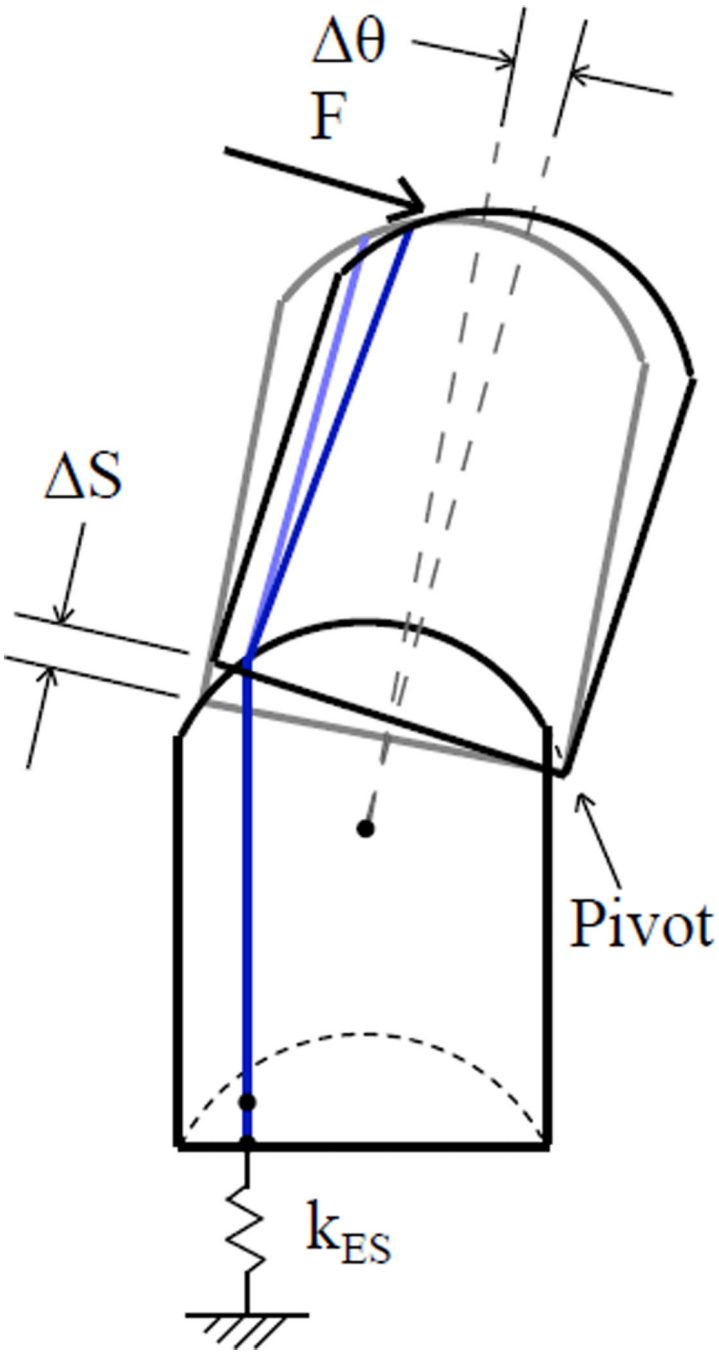

Fig. 6.
Elastic structural deformation kinematics.

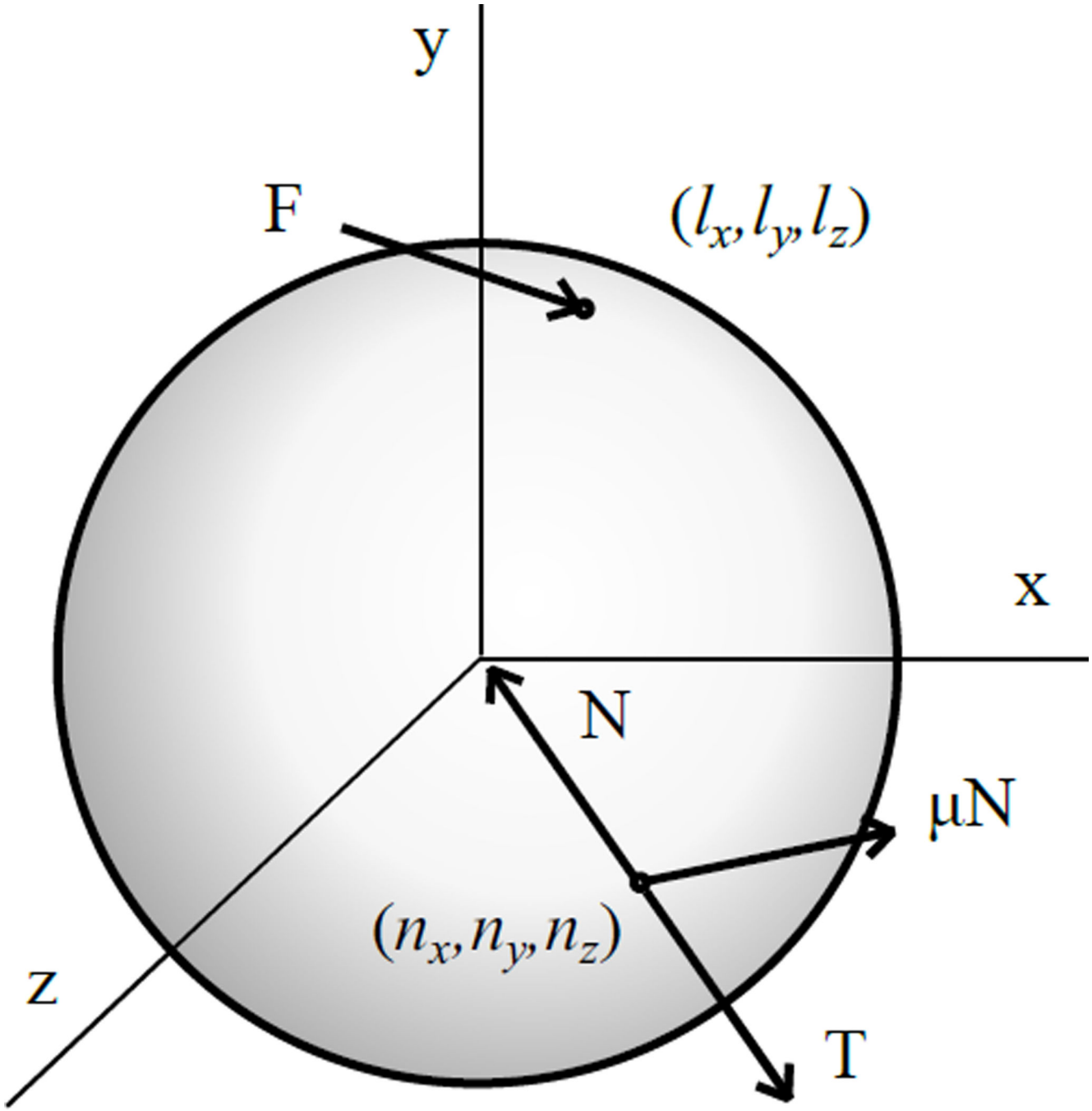

Fig. 7.
Diagram of forces acting during sliding displacement.

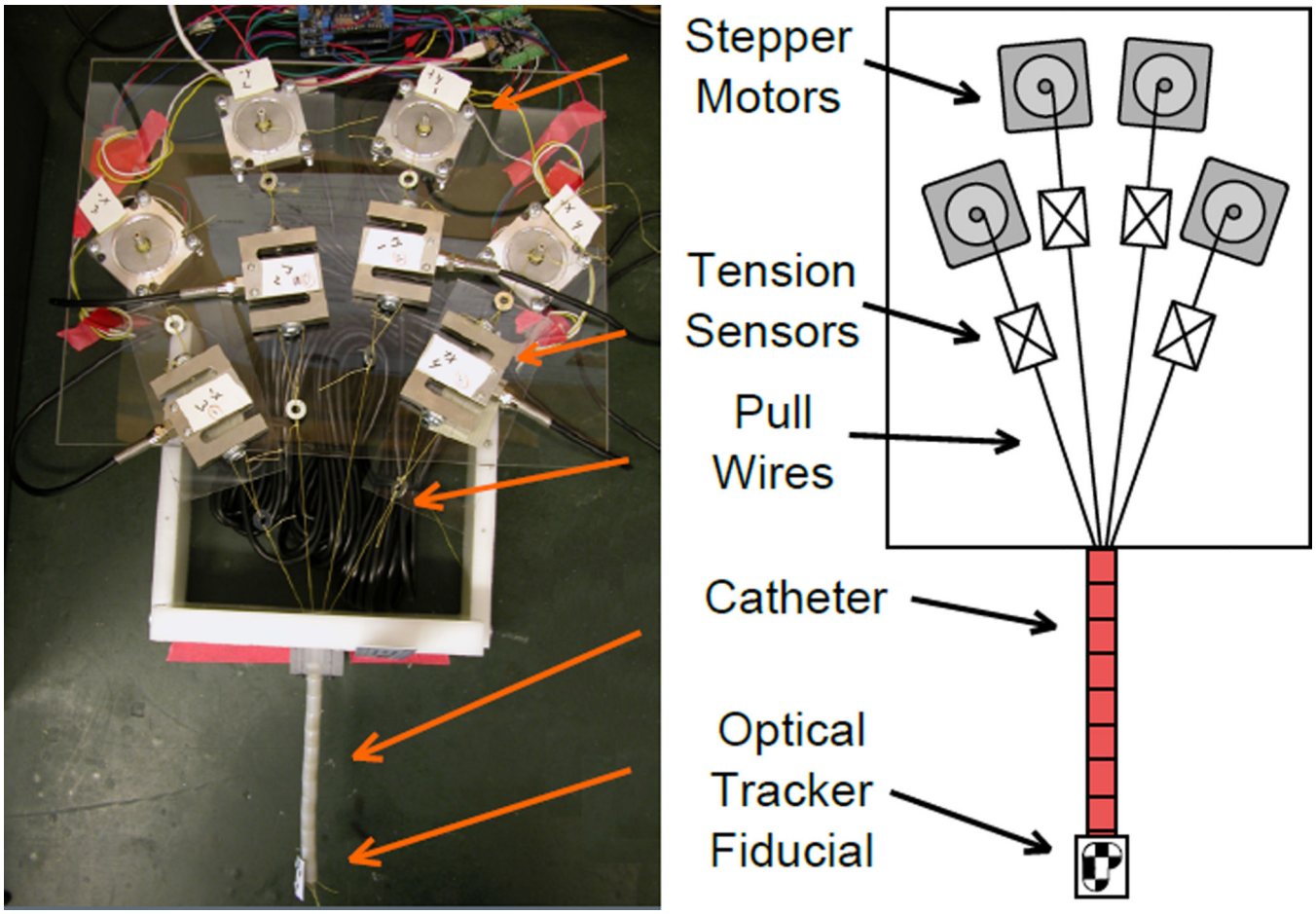

Fig. 8.
(*left*) Photo and (*right*) diagram of catheter stiffening robot system (view from top).

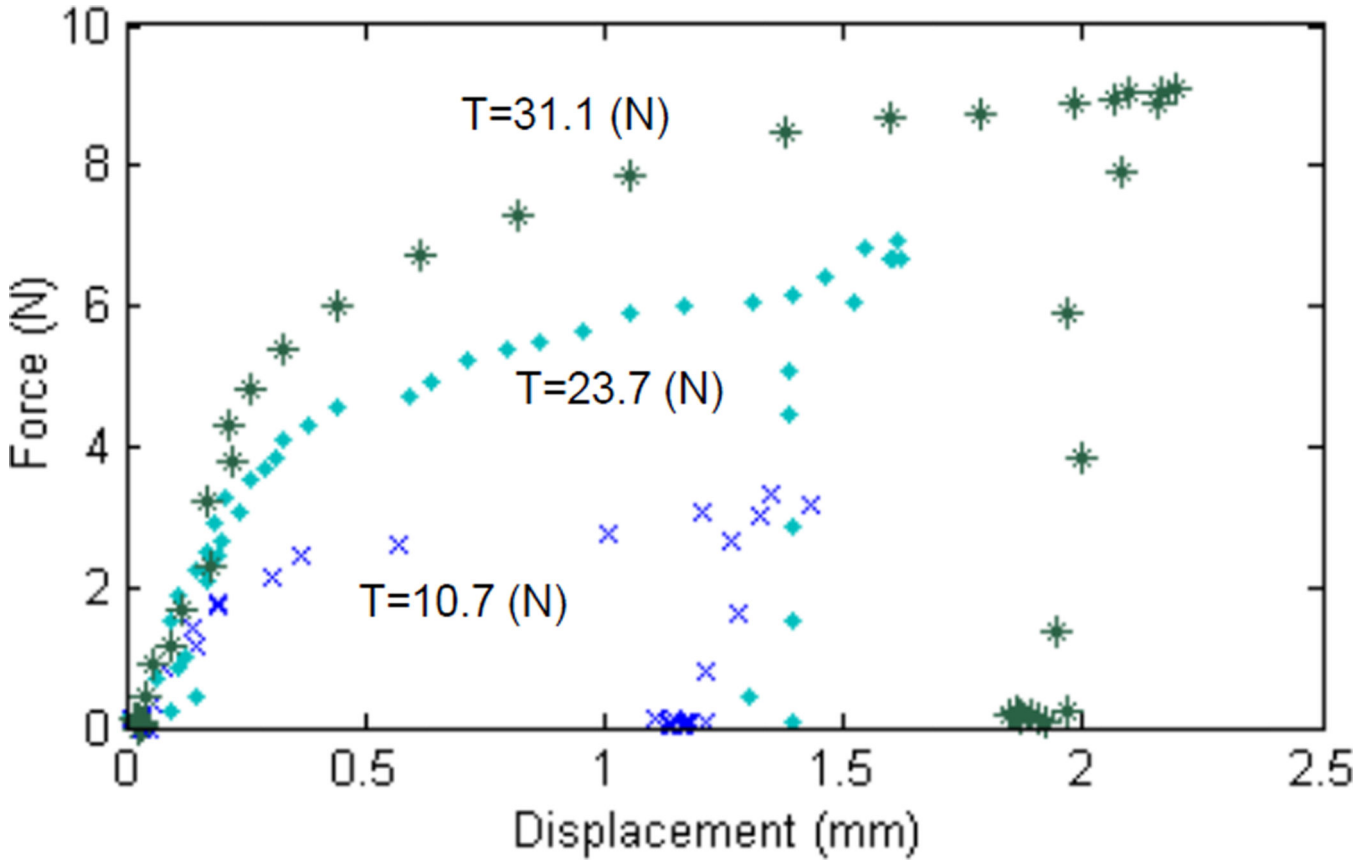

Fig. 9.
Moment applied to catheter tip creates sliding displacement for three different pull wire tensions.

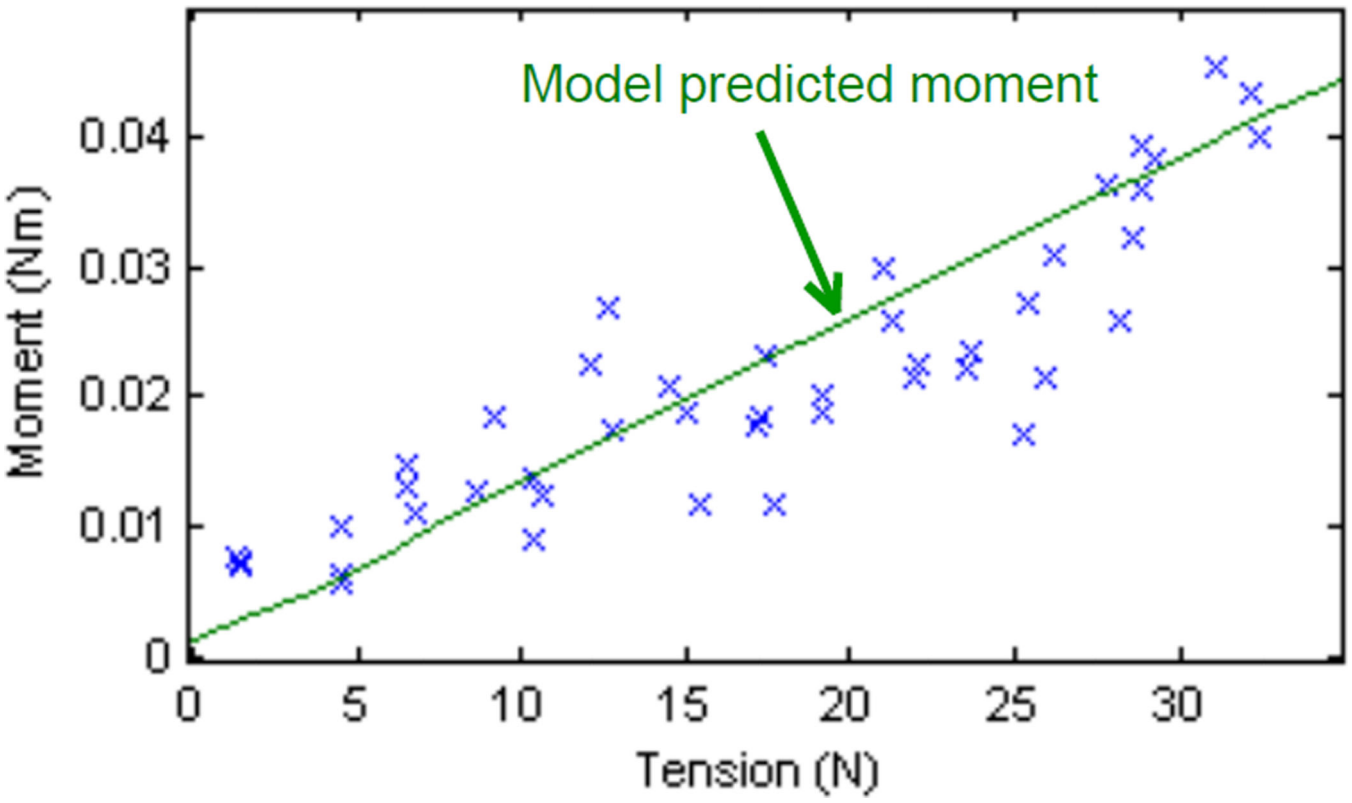

Fig. 10.

Moment applied to catheter tip creates sliding displacement as a function of the total pull wire tension. Line represents the model estimated moment to cause sliding.

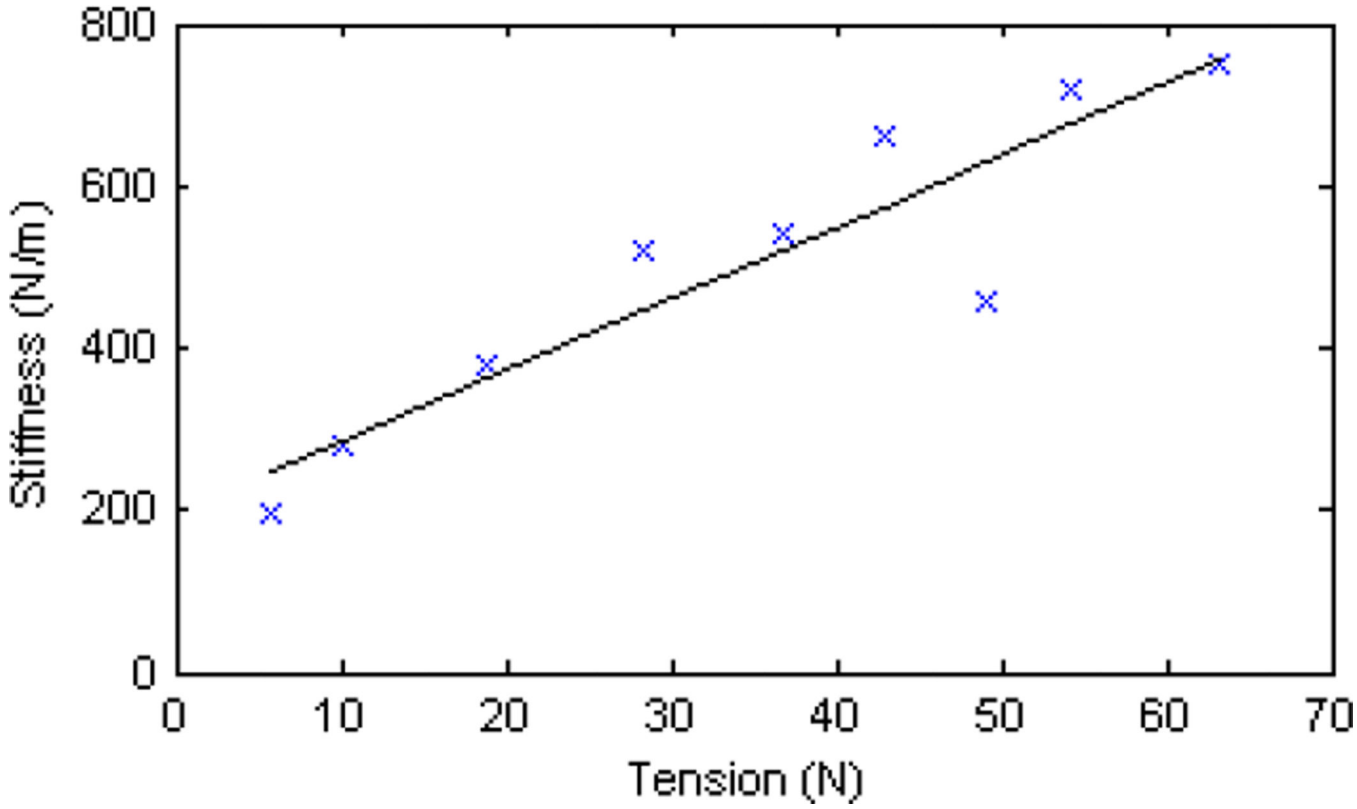

Fig. 11.

Overall catheter stiffness before sliding as a function of the total pull wire tension (10 vertebrae). Black line represents linear fit.